JCIM JOURNAL OF CHEMICAL INFORMATION AND MODELING

pubs.acs.org/jcim Article

Combined Structure and Ligand-Based Design of Selective Acetylcholinesterase Inhibitors

Horacio Pérez-Sánchez,* Helena den Haan, Alfonso Pérez-Garrido, Jorge Peña-García, Sandipan Chakraborty, Ilkay Erdogan Orhan,* Fatma Sezer Senol Deniz, and José Manuel Villalgordo*

Cite This: https://dx.doi.org/10.1021/acs.jcim.0c00463 Read Online

ACCESS | Metrics & More | Article Recommendations

ABSTRACT: Acetylcholinesterase is a prime target for therapeutic intervention in Alzheimer's disease. Acetylcholinesterase inhibitors (AChEIs) are used to improve cognitive abilities, playing therefore an important role in disease management. Drug repurposing screening has been performed on a corporate chemical library containing 11 353 compounds using a target fishing approach comprising three-dimensional (3D) shape similarity and pharmacophore modeling against an approved drug database, Drugbank. This initial screening identified 108 hits. Among them, eight molecules showed structural similarity to the known AChEI drug, pyridostigmine. Further structure-based screening using a pharmacophore-guided rescoring method identifies one more potential hit. Experimental evaluations of the identified hits sieve out a highly selective AChEI scaffold. Further lead optimization using a substructure search approach identifies 24 new potential hits. Three of the 24 compounds (compounds 10b, 10h, and 10i) based on a 6-(2-(pyrrolidin-1-yl)pyrimidin-4-yl)-thiazolo[3,2-*a*]pyrimidine scaffold showed highly promising AChE inhibition ability with IC_{50} values of 13.10 ± 0.53, 16.02 ± 0.46, and 6.22 ± 0.54 μM, respectively. Moreover, these compounds are highly selective toward AChE. Compound 10i shows AChE inhibitory activity similar to a known Food and Drug Administration (FDA)-approved drug, galantamine, but with even better selectivity. Interaction analysis reveals that hydrophobic and hydrogen-bonding interactions are the primary driving forces responsible for the observed high affinity of the compound with AChE.

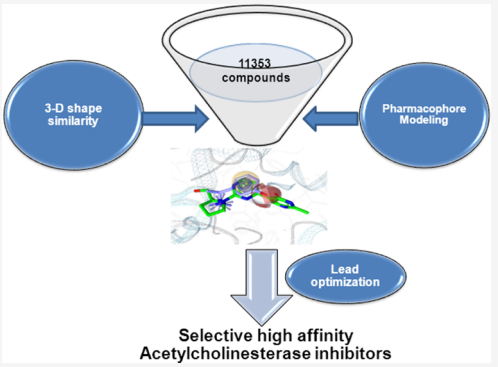

INTRODUCTION

Alzheimer's disease (AD) is a progressive neurodegenerative disorder, primarily in elderly people.[1] The pathophysiological features of the disease involve slow obliteration of cognition abilities, logical thinking, and sensory processes, which eventually lead to death.[1,2] Once considered a rare disorder, it now emerges as the fifth leading cause of death worldwide. Not only the severe morbidity rate but also the disease imposes a huge financial burden on the public health care system, which makes AD a primary health-care concern worldwide.

The past two decades witnessed tremendous growth in research interest to uncover disease pathogenesis and identify a therapy that can target the disease pathogenesis. Although several risk factors have been identified, the definitive cause of the disease remains elusive.[3] Early-onset AD follows a Mendelian pattern of inheritance, and mutations in *APP*, *PSEN1*, and *PSEN2* genes are strongly correlated with the disease prevalence.[4] Genes responsible for the late-onset AD, the most prevalent form, are not clearly identified. However, several risk factors have been identified. APOE ε4 allele shows a high risk of association with the prevalence of late-onset AD.[5−7] Genome-wide association studies (GWASs) have identified a sortilin-related receptor (*SORL1*) gene as a high-risk factor for AD.[8] Also, several susceptibility loci have been identified, and among them, *CLU*, *PICALM*, *CR1*, and *BIN1* genes are most significant.[9] Molecular characterization of the disease reveals a complex nature of disease pathogenesis due to the induction of many detrimental signaling cascades. Several signaling pathways including amyloid cascades,[3,10,11] neurofibrillary tangle formation,[12−15] cholinergic systems,[16−20] and oxidative stress-mediated processes[21−23] are induced simultaneously, and their cross-talk makes the disease pathogenesis highly complex and yet to be understood completely.

Neurochemical and histopathological studies of the brains of AD patients revealed a strong correlation between the degeneration of the presynaptic cholinergic system and the behavioral and cognition deficits.[20,24] Damage of the cholinergic neurotransmission, particularly in the region of the nucleus basalis of Meynert and medial septum, strongly

Received: May 1, 2020

https://dx.doi.org/10.1021/acs.jcim.0c00463
J. Chem. Inf. Model. XXXX, XXX, XXX−XXX

hampers different aspects of memory, cognition, behavior, and information processing by cortical and hippocampal regions.[17,20,24] Acetylcholine plays a crucial role in peripheral and central nervous systems.[25] Proper functioning of cholinergic neurotransmitters depends on the proper synchronization of the synthesis, storage, transportation, and degradation of acetylcholine.[25] The enzyme, acetylcholinesterase (AChE), degrades acetylcholine to generate choline and acetate. Reuptake of choline by the cholinergic neuron occurs through an active transport system. The enzyme colocalizes and firmly adheres to the senile plaque.[26,27] In the presence of bound AChE, the neurotoxicity of amyloid increases significantly.[28,29] All of these observations make AChE a prime target for therapeutic interventions in AD.[30−34] Notably, there is another enzyme that hydrolyzes acetylcholine, butyrylcholinesterase (BuChE). The activity of AChE decreases with the progression of AD pathogenesis,[35] while BChE activity progressively increases with disease progression.[36] This marked difference in their activities makes AChE a prime target for the treatment of early AD. However, in the advanced stage of AD, inhibition of BChE should provide a sustainable treatment. Most of the current Food and Drug Administration (FDA)-approved drugs for AD therapy are AChE inhibitors (AChEIs).[33] Donepezil, rivastigmine, and galantamine are clinically approved for palliative treatment in mild and moderate AD. However, all of these FDA-approved drugs are clinically limited due to their low selectivity and bioavailability and are also associated with moderate to severe side effects.[37] Reports of gastrointestinal anomalies and bradycardia are commonly associated with donepezil treatment,[38] whereas gastrointestinal side effects are also associated with both rivastigmine and galantamine treatments.[37] Therefore, the identification of novel safe and selective AChE inhibitors is an active research area. Several synthetic[39] and natural compounds have been shown to inhibit AChE;[40−43] however, receptor promiscuity severely hinders their applicability as drugs. Several pyridine derivatives[44−46] (tacrine and 7-methoxytacrine) also exhibit reversible AChE inhibition ability. Organophosphate groups of compounds[37,47] (ethyl parathion, malathion, phosmet, tabun, sarin, and many more), on the other hand, act as irreversible AChEIs. They are mostly used as insecticides and nerve agents. However, severe toxicity associated with the organophosphates, which occasionally lead to death, impede their clinical applications in AD.[48−50] Thus, exploration of new chemical scaffolds with reduced toxicity is still an active area of research. Recently, astaxanthin-*s*-allyl cysteine,[51] a sampangine derivative,[52] eugenol derivatives,[53] acridine-coumarin hybrids,[54] and flavonoids[40,55] have been shown to inhibit cholinesterases. The present work aims to identify novel selective AChEIs using a combination of structure- and ligand-based approaches.

Drug designing using cheminformatics can be classified as either target fishing or structure-based approaches. Target fishing is an approach to discover putative targets for a certain molecule. The efficacy of the target fishing approach can be further increased by combining several complementary methods. Pharmacophore modeling and three-dimensional (3D) shape similarity methods have been successfully used for the discovery of several bioactive compounds. On the other hand, if a structure of a macromolecule is available either using crystallography, NMR, cryo-EM, or using homology modeling or threading methods, then structure-based approaches are commonly used to find novel chemical modulators. Docking is the most commonly used structure-based method for the prediction of orientation and binding affinity of a molecule to the binding site of a macromolecule.

Transfer of therapeutics from the workbench to market is a slow process and associated with a huge cost. Most of the compounds fail in clinical trials. Drug repurposing is a viable alternative where novel therapeutic indications are identified from existing drugs.[56] Here, using a target fishing approach based on 3D shape similarity, pharmacophore modeling in combination with the structure-based drug design, we have identified a new selective acetylcholinesterase inhibitory (AChEI) scaffold exhibiting shape similarity to known drugs from the approved drug database, Drugbank.[57,58] Novel selective high-affinity AChEIs have been designed using a lead optimization approach for the treatment of Alzheimer's disease (AD). Activities of the identified leads are also validated using in vitro bioassays.

MATERIALS AND METHODS

Structure-Based Virtual Screening. The crystal structure of AChE was obtained from the Protein Data Bank with the accession code 1GQR.[59] It is a complex of AChE from an electric ray with an anti-Alzheimer's drug. Notably, the AChE of an electric eel is highly similar to the human AChE both in terms of sequence and structure, particularly the binding site is the same for human and electric ray AChE. The protonation state of the enzyme was predicted using Protoss.[60] All heteroatoms were removed from the crystal structure using Pymol. Dock prep tool available from Chimera v1.11.2[61] was used to prepare the receptor for docking by adding partial charges using the default parameters. Docking simulation was performed with Leadfinder v1.1.20.[62−64] Leadfinder is an efficient docking algorithm that combines a genetic algorithm with an effective local optimization procedure during the docking process. Three highly specialized accurate scoring functions have been implemented in the software. The benchmark studies show its ability to predict the binding poses as well as binding energies for highly diverse protein−ligand test sets.[62,64] An energy grid map of 30 $Å^3$ was selected and centered on the cocrystallized ligand. The 3D coordinate generation, defining the protonation state, removal of salts, and partial charge assignments were carried out for the compound library available from Villapharma using MolConverter with 3D fine parameters, and other parameters were kept by default. Postprocessing of docking poses was performed using Ligandscout v4.1.10[65] by a developed pharmacophore model based on the binding pose of rivastigmine in the crystal structure, 1GQR.

Ligand-Based Virtual Screening. The 3D shape similarity calculations were carried out using WEGA v2015[66] with pure shape as a parameter. 3D coordinate generation, salt removal, and assignment of partial charges for each compound of the library were carried out using the same protocol as mentioned above. For every compound, a pool of up to 100 conformations was generated using Cyndi with default parameters. The MMFF94 force field was used for partial charge calculations.

A pharmacophore model was then built for every compound labeled as approved in the DrugBank[58] database v4.2 using the espresso tool. For this purpose, two copies of each energy-minimized molecule were used as the training set for creating a model using the default parameters. The corporate database was then processed with the idbgen tool for creating up to 500

https://dx.doi.org/10.1021/acs.jcim.0c00463
J. Chem. Inf. Model. XXXX, XXX, XXX−XXX

Scheme 1. Synthesis of Key Intermediate (iii)

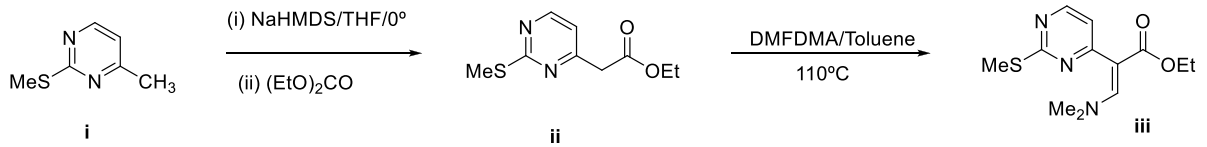

Scheme 2. Synthesis of Pyrimidinones (iv), Thiazolopyrimidinones (v), and Pyridopyrimidinones (vi)

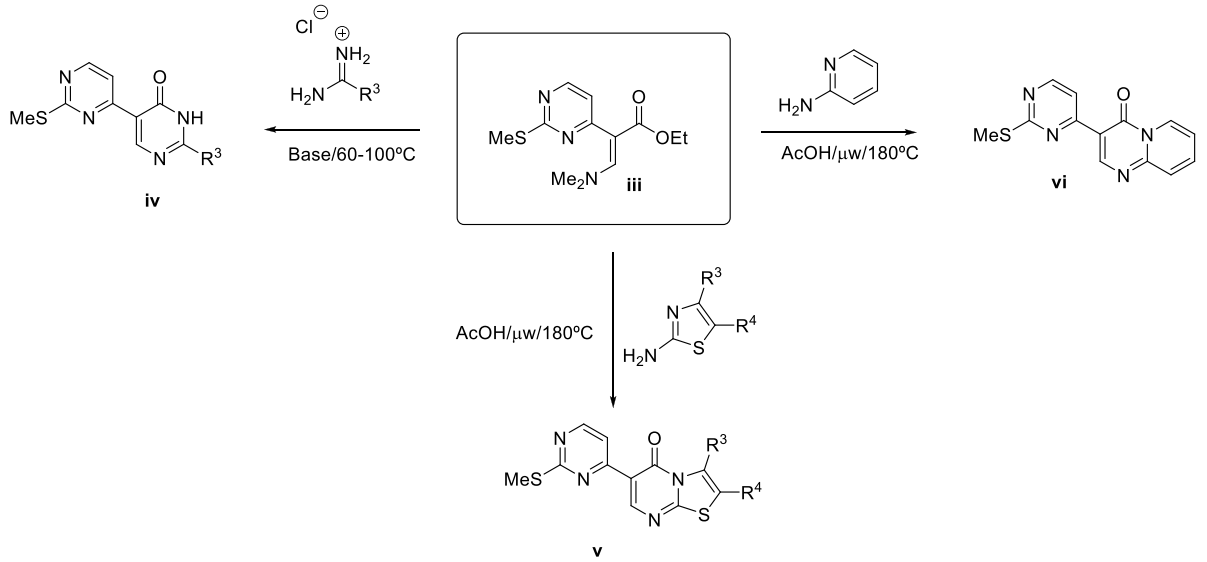

Scheme 3. Preparation of Compounds of Type 9, 10, and 11 from the Nucleophilic Displacement of the Sulfone Moieties in (vii), (viii), and (ix) with the Corresponding Pyrrolidines

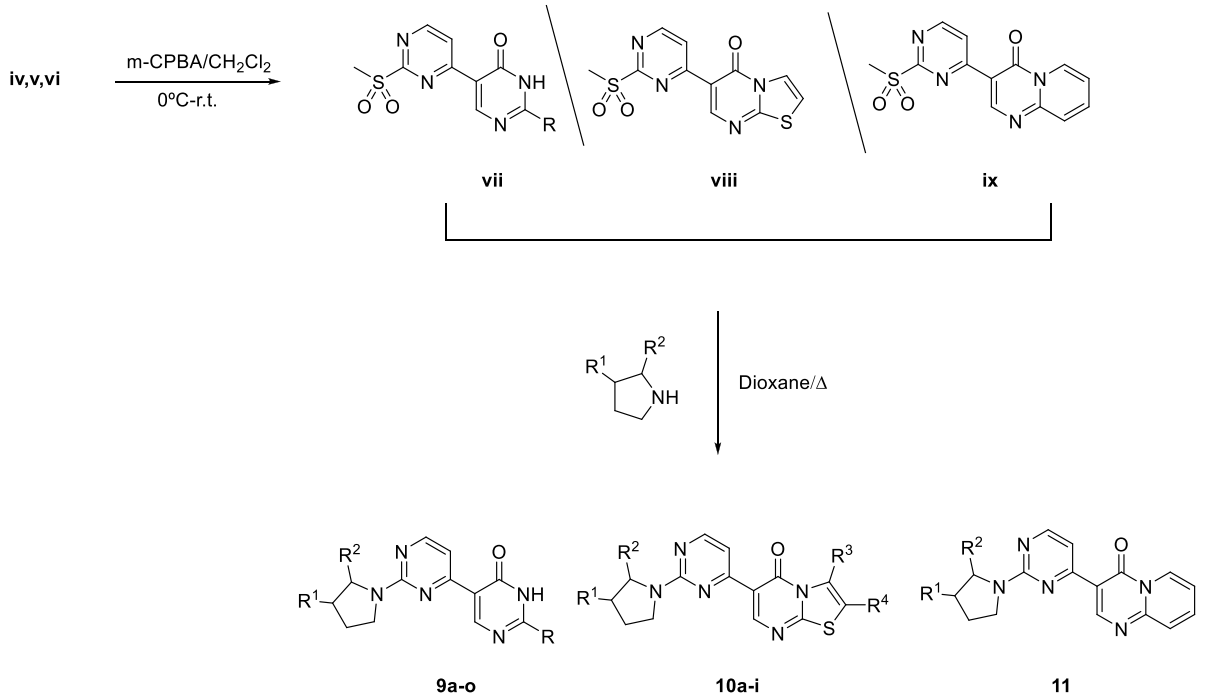

conformations for each molecule in the data set using the built-in omega conformer generator. The screening was performed with the iscreen[67] tool using the default parameters.

Quantitative Structure−Activity Relationship (QSAR) Analysis. We developed a QSAR model based on ISIDA Property Fragment Descriptors (IPLFDs)[68] to show the correlation of pharmacophoric properties with the activity. A total of 12 compounds with IC_{50} values in the molar concentration unit obtained from the in vitro bioassay were used to derive the QSAR. pIC_{50} ($-\log IC_{50}$) value was used as an activity value for each compound. An IPLFD was calculated for the major molecular species of each compound at pH 8.

https://dx.doi.org/10.1021/acs.jcim.0c00463
J. Chem. Inf. Model. XXXX, XXX, XXX−XXX

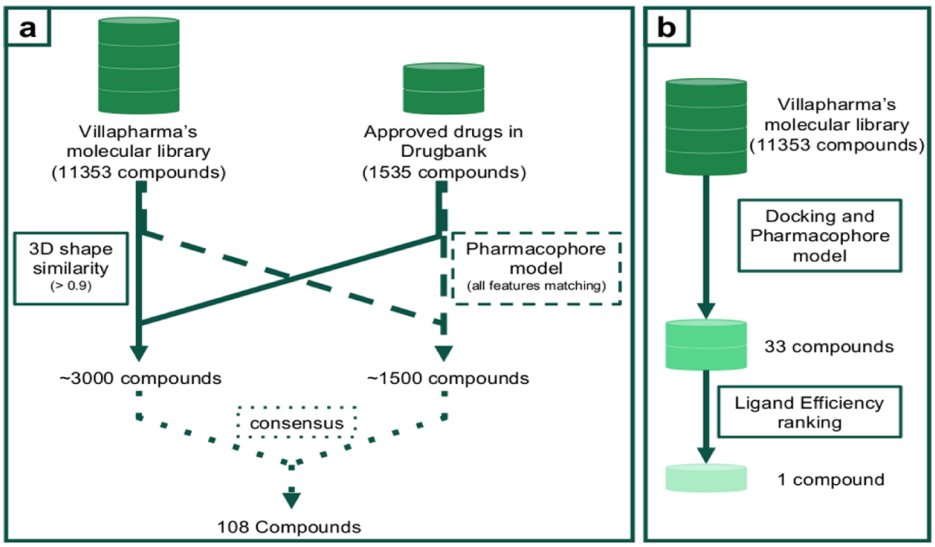

Figure 1. Virtual screening workflow for the screening of the corporate database. (a) Ligand-based methods and (b) structure-based method for AchEI identification.

Calculator plugins were used for microspecies prediction and atomic pharmacophoric labels calculation was carried out using Marvin 17.8.0, 2017, ChemAxon (http://www.chemaxon.com). Once the model was constructed, these descriptors can give a molecular contribution to the activity. A multilinear regression (MLR) was applied with an RSR variable selection for the development of a set of single QSAR models. We searched for models with 1 or 2 descriptors to ensure that the Topliss ratio was maintained. The goodness of fit for each model was assessed by examining the determination correlation coefficient (R^2), the standard deviation (s), and the Fisher ratio (F).

The robustness and predictive ability of the models were evaluated using cross-validation techniques by the leave-one-out (LOO) method, root-mean-squared error of prediction, and bootstrapping testing techniques (i.e., RMSEP, Q_{LOO}^2, and Q_{boot}^2). Further, the stability under heavy perturbations in the training set was checked by examining the outcome statistics of a response randomization procedure (Y-scrambling) based on the mean of Q^2 ($Q_{Yscr\text{-}mean}^2$) of each iteration (number of iteration = 300). All of these calculations were carried out using MATLAB (MATLAB 6.1, The MathWorks Inc., Natick, MA, 2000). The good quality of the models was judged by high F, low s, as well as the high values for R^2, Q_{LOO}^2 and Q_{boot}^2 and low values of RMSEP along with the $Q_{Yscr\text{-}mean}^2$ close to zero. The final model (consensus model) was obtained from the averaged predictions of four more distances (based on the canonical measure of distance (CMD)[69]) and predictive models (based on Q_{LOO}^2 and RMSEP).

General Synthetic Route toward Compounds of Type 9, 10, and 11. The synthesis of compounds of type 9, 10, and 11 was achieved from key intermediate (iii), as shown in Schemes 1 and 2. Thus, starting from commercially available 2-methylthiopyrimidine (i), a reaction with diethylcarbonate in the presence of a strong base afforded intermediate (ii). Subsequent reaction of (ii) with an excess of DMFDMA in refluxing toluene led to the formation of key intermediate (iii) (Scheme 1).

Key intermediate (iii) was then allowed to react with amidines or guanidines under basic conditions to afford pyrimidinone derivatives (iv). In turn, the reaction of (iii) with 2-aminothiazoles and 2-aminopyridines under acidic conditions led to 5*H*-thiazolo[3,2-*a*]pyrimidin-5-ones (v) and to 4*H*-pyrido[1,2-*a*]pyrimidin-4-ones (vi), respectively (Scheme 2).

Finally, oxidation of the methylthio moiety with m-CPBA of (iv), (v), and (vi) to the corresponding sulfones (vii), (viii), and (ix) and subsequent nucleophilic displacement with the corresponding pyrrolidines afforded the desired compound of types 9, 10, and 11 (Scheme 3).

AChE Inhibition Activity Assay. All of the compounds were obtained from the chemical repository of Villapharma. AChE and BChE inhibitory activities were measured by a slightly modified spectrophotometric method of Ellman.[70] Electric eel AChE (Type-VI-S; EC 3.1.1.7, Sigma, St. Louis, MO) and horse serum BChE (EC 3.1.1.8, Sigma, St. Louis, MO) were used, while acetylthiocholine iodide and butyrylthiocholine chloride (Sigma, St. Louis, MO) were used as the substrates of the reaction. 5,5′-Dithio-bis(2-nitrobenzoic)acid (DTNB; Sigma, St. Louis, MO) was used for the measurement of the anticholinesterase activity. All reagents and conditions were the same as described in our previous publication.[71] Briefly, 140 μL of sodium phosphate buffer (pH 8.0), 20 μL of DTNB, 20 μL of the test solution, and 20 μL of AChE/BChE solution were added by a multichannel automatic pipette (Gilson Pipetman, Paris, France) in a 96-well microplate and incubated for 15 min at 25 °C. The reaction was then initiated by the addition of 10 μL of acetylthiocholine iodide/butyrylthiocholine chloride. Hydrolysis of acetylthiocholine iodide/butyrylthiocholine chloride was monitored by the formation of yellow 5-thio-2-nitrobenzoate anion as a result of the reaction of DTNB with thiocholines, catalyzed by the enzymes, at 412 nm using a 96-well microplate reader (VersaMax Molecular Devices, Sunnyvale, CA). The measurements and calculations were evaluated using Softmax PRO 4.3.2.LS software (Sunnyvale, CA). The percentage of inhibition of AChE/BChE was determined by comparison of reaction rates of the samples relative to blank sample (ethanol in phosphate buffer pH = 8) using the formula $(E - S)/E \times 100$, where E is the activity of enzyme without test sample and S is the activity of the enzyme with the test sample. The

https://dx.doi.org/10.1021/acs.jcim.0c00463
J. Chem. Inf. Model. XXXX, XXX, XXX−XXX

Table 1. In Vitro Acetylcholinesterase (AChE) and Butyrylcholinesterase (BChE) Inhibitory Activity of the Initially Screened Compounds Obtained from Virtual Screening[a]

Compound id	Compound structure	AChE Inhibition (Inhibition% ± S.D.*) 100 μg/ml (IC_{50} in μM)	BChE Inhibition (Inhibition% ± S.D.*) 100 μg/ml (IC_{50} in μM)	Selectivity index ($AChE_{inhinition}$/ $BChE_{inhibition}$) 100 μg/ml
1	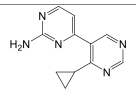	12.32 ± 1.54	4.90 ± 1.90	2.51
2	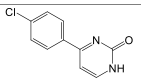	22.69 ± 3.03	28.65 ± 0.78	0.79
3	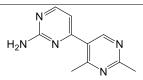	**	2.34 ± 1.02	-
4	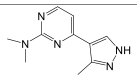	14.53 ± 1.67	17.70 ± 1.57	0.82
5	***	19.23 ± 0.57	-	-
6	***	27.94 ± 1.87	18.18 ± 1.87	1.53
7	***	33.22 ± 3.78	7.30 ± 1.16	4.55
8	***	4.45 ± 1.53	4.96 ± 2.86	0.89
9	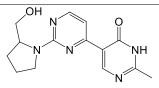	62.84 ± 0.92 (IC_{50}= 190.22 ±0.1)	17.12 ± 1.19	3.67
Galantamine HBr (Reference drug)	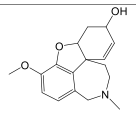	92.14±2.49 (IC_{50}= 2.52 ± 0.15)	81.93±2.52 (IC_{50}= 46.58±0.91)	2.51

[a]*Standard deviation; **no inhibition; ***confidential structure.

experiments were done in triplicate. Galanthamine (Sigma, St. Louis, MO) was used as the reference.

RESULTS AND DISCUSSION

Ligand-Based Virtual Screening. We chose the approved drug database available from Drugbank to identify a new compound with similar scaffolds from a corporative database (Villapharma) containing 11 353 compounds. Initial screening based on 3D shape comparison to each of the 1535 Drugbank compounds with a similarity threshold of 0.9 retrieves 2980 hits. Concurrently, pharmacophore-based screening has been performed on the corporative library using the models generated from the Drugbank compounds. To select a set of molecules with high shape similarity and pharmacophore fit values, we have crossed the results obtained by both the methodologies and retained only those compounds that meet both the criteria (Figure 1a). The consensus prediction results in 108 molecules from the database of Villapharma, which are predicted to be highly similar to 21 approved drugs. Among them, we have selected eight compounds for experimental characterization, which are chemically similar to pyridostigmine, a known cholinesterase inhibitor (compounds 1−8 in Table 1).

Structure-Based Virtual Screening. Furthermore, a structure-based approach has been adopted to mine new AChEIs (Figure 1b). The crystal structure of AChE, available from Protein Data Bank (accession code 1GQR[59]), has been used in the docking study. All of the compounds from the Villapharma compound library have been docked within the active site of AChE with Leadfinder v1.1.20.[62,63] For docking, a grid map of 30 $Å^3$ has been chosen and centered at the center of mass of the cocrystalized ligand. Postprocessing of the docking poses has been performed with the aid of Ligandscout v4.1.10[65] using a pharmacophore model of the bound

https://dx.doi.org/10.1021/acs.jcim.0c00463
J. Chem. Inf. Model. XXXX, XXX, XXX−XXX

rivastigmine, the native ligand of the AChE crystal structure. The success of molecular docking depends on two critical factors. These are the accuracy in predicting the binding pose and prediction of the binding affinities by different scoring functions. It has been found that docking programs can predict the correct binding pose with reasonable accuracy but not always a good docking conformation is related to a high scoring value.[72] Therefore, we adopted a different scoring method than the available force-field-based method. The resulting docking poses obtained for each ligand have been postscored using a structure-based pharmacophore model generated from the interaction of rivastigmine with AChE, derived using Ligandscout. The rationale behind the approach is that compounds with a predicted pose that fit within the binding site very similar to a known inhibitor must be highly scored. Docking-based screening is often inclined to the selection of compounds with higher molecular weight, thus normalizing the docking score with respect to the number of heavy atoms is proposed to discriminate between false and true positives. Therefore, we have opted for prioritizing the screened compound according to their predicted ligand efficiency (calculated as the docking score value by the number of heavy atoms). We have selected the top-ranked compound for further experimental validation (compound 9 in Table 1).

Lead Optimization. The inhibitory activities of the selected compounds have been verified using in vitro bioassay. Compounds 1−8 showed very low inhibition ability for both the cholinesterases, acetylcholinesterase (AChE) and butyrylcholinesterase (BChE). IC_{50} values were calculated only for compounds with an inhibition activity above 50%. Compound 9 ((*R*)-2-(2-(hydroxymethyl)pyrrolidin-1-yl)-2′-methyl-[4,5′-bipyrimidin]-4′(3′*H*)-one) exhibits a promising inhibitory activity for AChE, although its IC_{50} was still far from that of the reference compound, galantamine, a well-known FDA-approved AChEI. However, its selectivity is better than galanthamine. Molecular docking followed by pharmacophore fitting of the docked pose of compound 9 (green) to the pharmacophore model of rivastigmine (blue) shows that the binding of the compound to the AChE active site is nearly identical to the known drug, rivastigmine. Compound matches three out of the four features, namely, the aryl, hydrophobic, and hydrogen-bond acceptor groups (Figure 2).

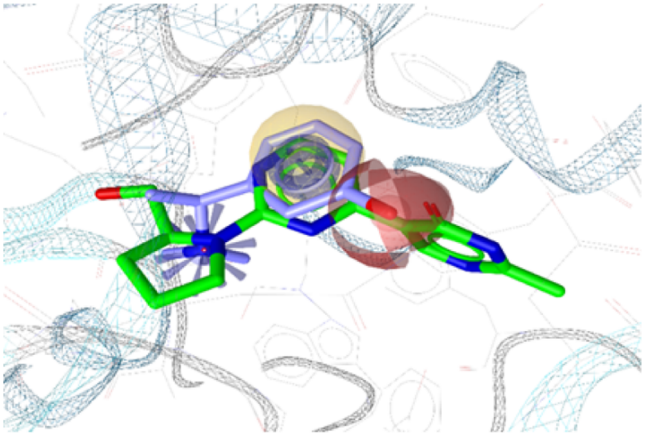

Figure 2. Fitting of the docked pose of compound 9 (green) to the pharmacophore model of bound rivastigmine (light blue). Pharmacophoric groups are highlighted.

Villapharma chemical library contains several analogues for each compound. Therefore, a lead optimization using substructure similarity search has been performed in the chemical library to mine new hits using the scaffold of the primary hit, compound 9. Twenty-four new hits have been identified with the scaffold of compound 9. These new molecules have been tested to measure their cholinesterase inhibitory activities (inhibition data are shown in Table 2). Among these, three molecules, 10b, 10h, and 10i, show inhibition ability comparable to the reference compound galantamine, as evident from Figure 3. Additionally, these compounds are selective to AChE, even the selectivity is better than the known inhibitor, galantamine.

Absolute configuration at the stereocenter for each scaffold is shown below

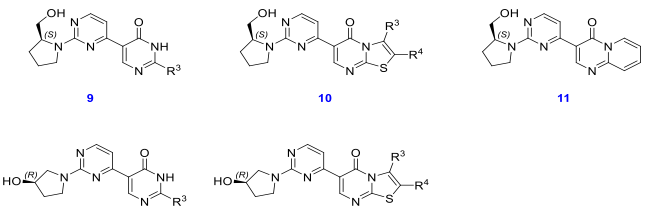

We have further developed the QSAR model to understand the critical determinants of AChEI activity, which can be used to design compounds with improved activity. Four QSAR models were selected to make a consensus model for structural interpretation (Table 3).

The equation of the $QSAR_1$ model with the statistical parameters is shown below

$$pIC_{50} = 0.815\cdot h002 - r007 - r009 + 0.669\cdot a009 - h004 - h007;\ R^2 = 0.823;\ Q^2_{LOO} = 0.747;\ Q^2_{Yscr-mean} = -0.666;\ RMSEP = 0.308;\ Q^2_{boot} = 0.658;\ F = 20.92;\ s = 0.25;\ Q^2_{LMO} = 0.783$$

where h002-r007-r009 and a009-h004-h007 represent the fuzzy pharmacophore triplets codes. The letters codify the type of a pharmacophoric atom (h, hydrophobic; r, aromatic; a, hydrogen-bond acceptor), and the number is the topologic distance between them.

The pharmacophoric contribution chart (Figure 4) is derived from the model coefficients and the pharmacophoric properties included in the descriptors codes. This figure shows that hydrogen-bond donor groups in the molecule affect negatively and hydrophobicity, aromaticity, and hydrogen-bond acceptor groups have a positive influence on the affinity.

Figure 5 shows the contributions imprinted on the most active chemical and one of the compounds with lower activity (compound 9a, Table 2). It seems that the low activity of the compound 9a is due to the presence of the hydrogen-bond donor nitrogen in the pyrimidone ring (negative contribution) and the absence of the thiazoline ring (increase in aromaticity/hydrophobic atoms).

CONCLUSIONS

The cholinergic system plays a crucial role in the proper functioning of memory, cognition, and behavior.[25] In Alzheimer's disease (AD), the cholinergic neurotransmission is severely hampered.[16,20,24,73] Acetylcholine is a neurotransmitter that plays an integral part in the cholinergic system. Acetylcholinesterase (AChE) degrades acetylcholine to

https://dx.doi.org/10.1021/acs.jcim.0c00463
J. Chem. Inf. Model. XXXX, XXX, XXX−XXX

Table 2. Inhibitory Activity for AChE and BChE of Compounds Extracted Using the Scaffold of Compound 9[a]

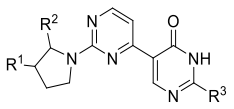

2-(pyrrolidin-1-yl)-[4,5'-bipyrimidin]-4'(3'*H*)-ones

9a-o

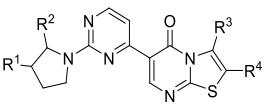

6-(2-(pyrrolidin-1-yl)pyrimidin-4-yl) -5*H*-thiazolo[3,2-*a*]pyrimidin-5-ones

10a-i

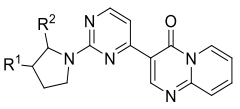

3-(2-(pyrrolidin-1-yl)pyrimidin-4-yl)-4*H*-pyrido[1,2-*a*]pyrimidin-4-one

11

Compound ID	R groups	AChE Inhibition (% ± S.D.*) 100 μg/ml (IC_{50}, μM)	BChE Inhibition (% ± S.D.*) 100 μg/ml (IC_{50}, μM)	Selectivity index ($AChE_{inhinition}$/ $BChE_{inhibition}$)
(9a)	R_1 = H R_2 = CH_2OH R_3 = CH_3	55.96±2.67 (IC_{50}=294±5.09)	19.73±1.70	2.83
(9b)	R_1 = H R_2 = CH_2OH R_3= 	75.55±2.28 (IC_{50}=73.33±3.2)	88.86±1.64 (IC_{50}=31.06±0.8)	0.85
(9c)	R_1 = H R_2 = CH_2OH R_3 = 	26.66±2.24	7.56±1.78	3.52
(9d)	R_1 = H R_2 = CH_2OH R_3= 	27.99±1.70	9.28±1.71	3.01
(9e)	R_1 = H R_2 = CH_2OH R_3 = 	3.99±0.76	19.41±3.12	0.20
(9f)	R_1 = H R_2 = CH_2OH R_3 = 	**	21.77±2.11	-
(9g)	R_1 = H R_2 = H R_3 = 	30.91±0.91	24.92±3.15	1.24

https://dx.doi.org/10.1021/acs.jcim.0c00463
J. Chem. Inf. Model. XXXX, XXX, XXX−XXX

Table 2. continued

Compound ID	R groups	AChE Inhibition (% ± S.D.*) 100 μg/ml ($IC_{50,}$ μM)	BChE Inhibition (% ± S.D.*) 100 μg/ml ($IC_{50,}$ μM)	Selectivity index ($AChE_{inhinition}$/ $BChE_{inhibition}$)
(9h)	R_1 = OH R_2 = H R_3 = 	-	17.91±0.09	-
(9i)	R_1 = OH R_2 = H R_3 = 	-	9.81±2.32	-
(9j)	R_1 = H R_2 = H R_3 = 	14.69±0.24	17.90±2.81	0.82
(9k)	R_1 = H R_2 = CH_2OH R_3 = 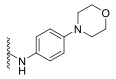	59.07±2.72 (IC_{50}=146.97±7.1)	22.54±3.85	2.62
(9l)	R_1 = OH R_2 = H R_3 = 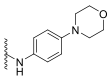	11.00±0.89	18.26±1.25	0.60
(9m)	R_1 = H R_2 = H R_3 = 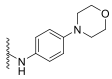	50.49±3.86	13.90±1.93	3.63
(9n)	R_1 = H R_2 = H R_3 = 	23.81±2.82	6.93±2.44	3.43
(9o)	R_1 = OH R_2 = H R_3 = 	19.44±3.61	10.47±2.93	1.85
(10a)	R_1 = H R_2 = CH_2OH R_3 = H R_4 = H	83.09±2.56 (IC_{50}=35.22±4.04)	26.22±3.95	3.16

https://dx.doi.org/10.1021/acs.jcim.0c00463
J. Chem. Inf. Model. XXXX, XXX, XXX−XXX

Table 2. continued

Compound ID	R groups	AChE Inhibition (% ± S.D.*) 100 μg/ml ($IC_{50,}$ μM)	BChE Inhibition (% ± S.D.*) 100 μg/ml ($IC_{50,}$ μM)	Selectivity index ($AChE_{inhinition}$/ $BChE_{inhibition}$)
(10b)	R_1 = H R_2 = CH_2OH R_3 = H R_4 = CH_3	91.14±0.96 (IC_{50}=13.10±0.53)	34.65±2.94	2.63
(10c)	R_1 = H R_2 = H R_3 = H R_4 = CH_3	78.66±3.43 (IC_{50}=36.48±2.52)	17.56±0.64	4.47
(10d)	R_1 = H R_2 = H R_3 = H R_4 = H	48.80±2.43	12.93±2.16	3.77
(10e)	R_1 = OH R_2 = H R_3 = H R_4 = CH_3	81.15±4.42 (IC_{50}=54.16±1.21)	21.23±3.66	3.82
(10f)	R_1 = OH R_2 = H R_3 = H R_4 = H	50.91±1.60 (IC_{50}=368.75±5.44)	8.56±1.12	5.94
(10g)	R_1 = OH R_2 = H R_3 = H R_4 = Cl	54.31±0.85 (IC_{50}=194.10±2.8)	12.37±3.61	4.39
(10h)	R_1 = H R_2 = H R_3 = CH_3 R_4 = H	94.02±1.30 (IC_{50}=16.02±0.46)	40.45±3.73	2.32

https://dx.doi.org/10.1021/acs.jcim.0c00463
J. Chem. Inf. Model. XXXX, XXX, XXX−XXX

Table 2. continued

Compound ID	R groups	AChE Inhibition (% ± S.D.*) 100 μg/ml ($IC_{50,}$ μM)	BChE Inhibition (% ± S.D.*) 100 μg/ml ($IC_{50,}$ μM)	Selectivity index ($AChE_{inhinition}$/ $BChE_{inhibition}$)
(10i)	R_1 = H R_2 = CH_2OH R_3 = CH_3 R_4 = H	86.43±3.11 (IC_{50}=6.22±0.54)	31.81±0.71	2.71
(11)	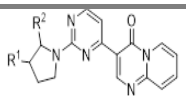	83.27±1.62 (IC_{50}=51.17±0.54)	36.02±3.78	2.31
Galantamine HBr	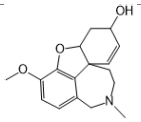	92.14±2.49 (IC_{50}=2.52±0.15)	81.93±2.52 (IC_{50}=46.58±0.91)	1.12

[a]Stereochemistry: compounds 9a, 9b, 9c, 9d, 9e, 9f, and 9k have the absolute configuration (*S*); compounds 9g, 9j, 9m, and 9n are achiral; and compounds 9h, 9i, 9l, and 9o have the absolute configuration (*R*). Compounds 10a, 10b, and 10i have the absolute configuration (*S*); compounds 10c, 10d, and 10h are achiral; and compounds 10e, 10f, and 10g have the absolute configuration (*R*). Compound 11 has an absolute configuration (*S*).

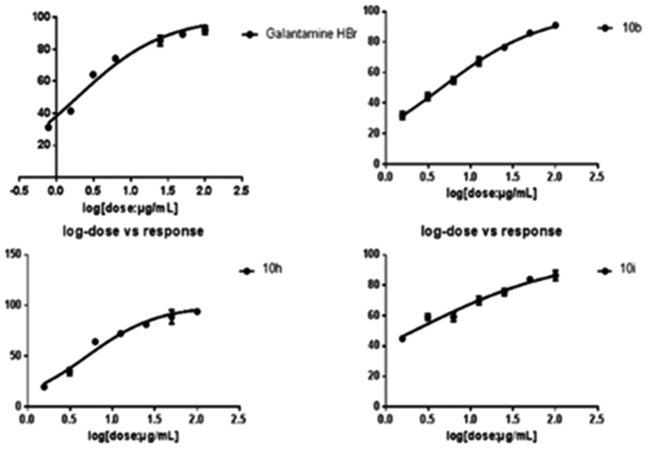

Figure 3. AChE inhibition curves for the three most potent inhibitors of the series and galantamine HBr are shown.

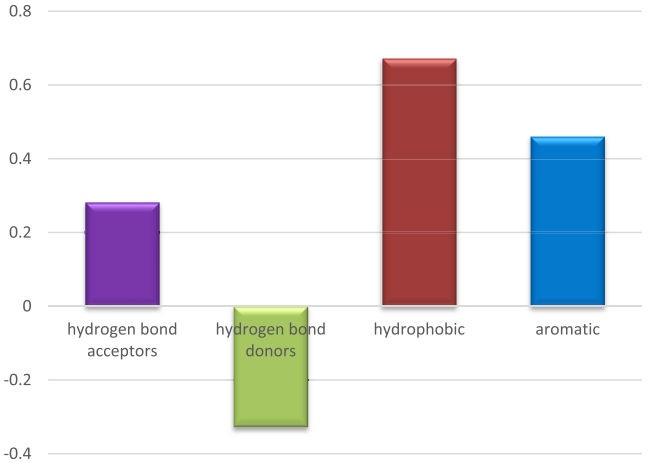

Figure 4. Pharmacophore contributions of the molecule to the activity.

generate choline and acetate. Therefore, AChE inhibitor designing is a topic of huge research interest.[30−33,40,43,74,75] In fact, most of the currently FDA-approved drugs for moderate to severe AD are AChE inhibitors (AChEIs); however, these drugs are associated with moderate to severe side effects. Therefore, the identification of novel AChE inhibitory scaffolds is an active area of research. Several synthetic and natural compounds have been identified that

Table 3. Statistical Parameters Associated with the Four Selected Qsar Models and the Derived Consensus Model

	descriptor no.	R^2	Q_{LOO}^2	$Q_{Yscr\_mean}^2$	RMSEP	Q_{boot}^2	*F*	s
$QSAR_1$	2	0.823	0.747	−0.666	0.308	0.658	20.92	0.25
$QSAR_2$	2	0.855	0.788	−0.726	0.319	0.773	26.51	0.227
$QSAR_3$	2	0.847	0.777	−0.668	0.213	0.776	24.88	0.233
$QSAR_4$	2	0.854	0.767	−0.525	0.309	0.758	26.32	0.227
consensus		0.903	0.871	−0.432	0.160	0.755		

https://dx.doi.org/10.1021/acs.jcim.0c00463
J. Chem. Inf. Model. XXXX, XXX, XXX−XXX

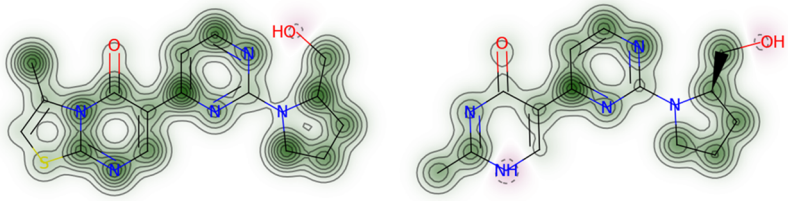

Figure 5. Structures of compound 10i (pIC_{50} = 5.209) and compound 9a (pIC_{50} = 3.521) with their atomic contribution to the activity. Green = positive contribution; red = negative contribution.

show inhibition of AChE in vitro.[30,31,39,40,43,74,76] However, most of the compound fails in the clinical trials due to their undesirable side effects. Drug repurposing emerges as a potential alternative, where new therapeutic indications are identified for the currently approved drugs. This motivates us to undertake the designing initiative to identify novel AChE inhibitors with a structural scaffold of existing drugs. Initially, a multitier target fishing approach combining pharmacophore modeling and 3D similarity searches has been opted to identify novel lead AChEI from the Villapharma compound library with a scaffold of approved drugs. Further lead optimization using a substructure search screened three highly selective AChE inhibitors comprising a 6-(2-(pyrrolidin-1-yl)pyrimidin-4-yl)-thiazolo[3,2-*a*]pyrimidine skeleton with the IC_{50} values of 13.10 ± 0.53, 16.02 ± 0.46, and 6.22 ± 0.54 μM. To the best of our knowledge, the reported scaffolds are novel. We also would like to emphasize that each computational method was developed with definite assumptions. Therefore, each method has its advantage and disadvantage. Therefore, it is often wise to interpret results in terms of consensus prediction, which reduced the chance of false positive. Here, we have demonstrated how we can integrate different computational methods in lead discovery. The approach adopted in the present study is promising in lead discovery based on the drug repurposing approach and opens the door for therapeutic discovery for other complex diseases too.

AUTHOR INFORMATION

Corresponding Authors

Horacio Pérez-Sánchez − *Structural Bioinformatics and High Performance Computing Group (BIO-HPC), Universidad Católica San Antonio de Murcia (UCAM), Guadalupe 30107, Spain*; orcid.org/0000-0003-4468-7898; Email: hperez@ucam.edu

Ilkay Erdogan Orhan − *Department of Pharmacognosy, Faculty of Pharmacy, Gazi University, 06330 Ankara, Turkey*; Email: iorhan@gazi.edu.tr

José Manuel Villalgordo − *Parque Tecnológico de Fuente Álamo, Villapharma Research, 30320 Murcia, Spain*; Email: JoseManuelVillalgordo@eurofins.com

Authors

Helena den Haan − *Structural Bioinformatics and High Performance Computing Group (BIO-HPC), Universidad Católica San Antonio de Murcia (UCAM), Guadalupe 30107, Spain; Parque Tecnológico de Fuente Álamo, Villapharma Research, 30320 Murcia, Spain*

Alfonso Pérez-Garrido − *Structural Bioinformatics and High Performance Computing Group (BIO-HPC), Universidad Católica San Antonio de Murcia (UCAM), Guadalupe 30107, Spain*; orcid.org/0000-0002-3141-1086

Jorge Peña-García − *Structural Bioinformatics and High Performance Computing Group (BIO-HPC), Universidad Católica San Antonio de Murcia (UCAM), Guadalupe 30107, Spain*

Sandipan Chakraborty − *Amity Institute of Biotechnology, Amity University, Kolkata 700135, India*; orcid.org/0000-0001-8759-1074

Fatma Sezer Senol Deniz − *Department of Pharmacognosy, Faculty of Pharmacy, Gazi University, 06330 Ankara, Turkey*; orcid.org/0000-0002-5850-9841

Complete contact information is available at: https://pubs.acs.org/10.1021/acs.jcim.0c00463

Notes

The authors declare no competing financial interest.

ACKNOWLEDGMENTS

This work was funded by a grant from the Spanish Ministry of Economy and Competitiveness (CTQ2017-87974-R) and the Fundación Séneca del Centro de Coordinación de la Investigación de la Region′ de Murcia under Projects 20988/PI/18 and 20524/PDC/18. This research was partially supported by the supercomputing infrastructure of Poznan Supercomputing Center, the e-infrastructure program of the Research Council of Norway, the supercomputer center of UiT—the Arctic University of Norway, and the computing facilities of Extremadura Research Centre for Advanced Technologies (CETA—CIEMAT), funded by the European Regional Development Fund (ERDF). CETA—CIEMAT belongs to CIEMAT and the Government of Spain. The authors also acknowledge the computing resources and technical support provided by the Plataforma Andaluza de Bioinformática of the University of Málaga. Powered@NLHPC research was partially supported by the supercomputing infrastructure of NLHPC (ECM-02).

REFERENCES

(1) Selkoe, D. J. The molecular pathology of Alzheimer's disease. *Neuron* **1991**, *6*, 487−498.

(2) Roberson, E. D.; Mucke, L. 100 years and counting: prospects for defeating Alzheimer's disease. *Science* **2006**, *314*, 781−784.

(3) Sandipan, C. Multi-potent Natural Scaffolds Targeting Amyloid Cascade: In Search of Alzheimer's Disease Therapeutics. *Curr. Top. Med. Chem.* **2017**, *17*, 3336−3348.

(4) Krüger, J.; Moilanen, V.; Majamaa, K.; Remes, A. M. Molecular Genetic Analysis of the APP, PSEN1, and PSEN2 Genes in Finnish Patients With Early-onset Alzheimer Disease and Frontotemporal Lobar Degeneration. *Alzheimer Dis. Assoc. Disord.* **2012**, *26*, 272−276.

https://dx.doi.org/10.1021/acs.jcim.0c00463
J. Chem. Inf. Model. XXXX, XXX, XXX−XXX

(5) Schmechel, D. E.; Saunders, A. M.; Strittmatter, W. J.; Crain, B. J.; Hulette, C. M.; Joo, S. H.; Pericak-Vance, M. A.; Goldgaber, D.; Roses, A. D. Increased amyloid beta-peptide deposition in cerebral cortex as a consequence of apolipoprotein E genotype in late-onset Alzheimer disease. *Proc. Natl. Acad. Sci. U.S.A.* **1993**, *90*, 9649−9653.
(6) Panza, F.; Frisardi, V.; Seripa, D.; D'Onofrio, G.; Santamato, A.; Masullo, C.; Logroscino, G.; Solfrizzi, V.; Pilotto, A. Apolipoprotein E genotypes and neuropsychiatric symptoms and syndromes in late-onset Alzheimer's disease. *Ageing Res. Rev.* **2012**, *11*, 87−103.
(7) D'Onofrio, G.; Panza, F.; Seripa, D.; Sancarlo, D.; Paris, F.; Cascavilla, L.; Urbano, M.; Gravina, C.; Fontana, A.; Solfrizzi, V.; Pellegrini, F.; Pilotto, A. The APOE polymorphism in Alzheimer's disease patients with neuropsychiatric symptoms and syndromes. *Int. J. Geriatr. Psychiatry* **2011**, *26*, 1062−1070.
(8) Rogaeva, E.; Meng, Y.; Lee, J. H.; Gu, Y.; Kawarai, T.; Zou, F.; Katayama, T.; Baldwin, C. T.; Cheng, R.; Hasegawa, H.; Chen, F.; Shibata, N.; Lunetta, K. L.; Pardossi-Piquard, R.; Bohm, C.; Wakutani, Y.; Cupples, L. A.; Cuenco, K. T.; Green, R. C.; Pinessi, L.; Rainero, I.; Sorbi, S.; Bruni, A.; Duara, R.; Friedland, R. P.; Inzelberg, R.; Hampe, W.; Bujo, H.; Song, Y.-Q.; Andersen, O. M.; Willnow, T. E.; Graff-Radford, N.; Petersen, R. C.; Dickson, D.; Der, S. D.; Fraser, P. E.; Schmitt-Ulms, G.; Younkin, S.; Mayeux, R.; Farrer, L. A.; St George-Hyslop, P. The neuronal sortilin-related receptor SORL1 is genetically associated with Alzheimer disease. *Nat. Genet.* **2007**, *39*, 168−177.
(9) Seshadri, S.; Fitzpatrick, A. L.; Ikram, M. A.; DeStefano, A. L.; Gudnason, V.; Boada, M.; Bis, J. C.; Smith, A. V.; Carassquillo, M. M.; Lambert, J. C.; Harold, D.; Schrijvers, E. M.; Ramirez-Lorca, R.; Debette, S.; Longstreth, W. T., Jr.; Janssens, A. C.; Pankratz, V. S.; Dartigues, J. F.; Hollingworth, P.; Aspelund, T.; Hernandez, I.; Beiser, A.; Kuller, L. H.; Koudstaal, P. J.; Dickson, D. W.; Tzourio, C.; Abraham, R.; Antunez, C.; Du, Y.; Rotter, J. I.; Aulchenko, Y. S.; Harris, T. B.; Petersen, R. C.; Berr, C.; Owen, M. J.; Lopez-Arrieta, J.; Varadarajan, B. N.; Becker, J. T.; Rivadeneira, F.; Nalls, M. A.; Graff-Radford, N. R.; Campion, D.; Auerbach, S.; Rice, K.; Hofman, A.; Jonsson, P. V.; Schmidt, H.; Lathrop, M.; Mosley, T. H.; Au, R.; Psaty, B. M.; Uitterlinden, A. G.; Farrer, L. A.; Lumley, T.; Ruiz, A.; Williams, J.; Amouyel, P.; Younkin, S. G.; Wolf, P. A.; Launer, L. J.; Lopez, O. L.; van Duijn, C. M.; Breteler, M. M. CHARGE Consortium; GERAD1 Consortium; EADI1 Consortium. Genome-wide analysis of genetic loci associated with alzheimer disease. *J. Am. Med. Assoc.* **2010**, *303*, 1832−1840.
(10) Suh, Y.-H.; Checler, F. Amyloid Precursor Protein, Presenilins, and α-Synuclein: Molecular Pathogenesis and Pharmacological Applications in Alzheimer's Disease. *Pharmacol. Rev.* **2002**, *54*, 469−525.
(11) Karran, E.; Mercken, M.; De Strooper, B. The amyloid cascade hypothesis for Alzheimer's disease: an appraisal for the development of therapeutics. *Nat. Rev. Drug Discov.* **2011**, *10*, 698−712.
(12) Noble, W.; Olm, V.; Takata, K.; Casey, E.; Mary, O.; Meyerson, J.; Gaynor, K.; LaFrancois, J.; Wang, L.; Kondo, T.; Davies, P.; Burns, M.; Veeranna; Nixon, R.; Dickson, D.; Matsuoka, Y.; Ahlijanian, M.; Lau, L. F.; Duff, K. Cdk5 is a key factor in tau aggregation and tangle formation in vivo. *Neuron* **2003**, *38*, 555−565.
(13) Götz, J.; Schild, A.; Hoerndli, F.; Pennanen, L. Amyloid-induced neurofibrillary tangle formation in Alzheimer's disease: insight from transgenic mouse and tissue-culture models. *Int. J. Dev. Neurosci.* **2004**, *22*, 453−465.
(14) Boutajangout, A.; Quartermain, D.; Sigurdsson, E. M. Immunotherapy targeting pathological tau prevents cognitive decline in a new tangle mouse model. *J. Neurosci.* **2010**, *30*, 16559−16566.
(15) Asuni, A. A.; Boutajangout, A.; Quartermain, D.; Sigurdsson, E. M. Immunotherapy targeting pathological tau conformers in a tangle mouse model reduces brain pathology with associated functional improvements. *J. Neurosci.* **2007**, *27*, 9115−9129.
(16) Sims, N. R.; Bowen, D. M.; Allen, S. J.; Smith, C. C. T.; Neary, D.; Thomas, D. J.; Davison, A. N. Presynaptic Cholinergic Dysfunction in Patients with Dementia. *J. Neurochem.* **1983**, *40*, 503−509.
(17) Maurer, S. V.; Williams, C. L. The Cholinergic System Modulates Memory and Hippocampal Plasticity via Its Interactions with Non-Neuronal Cells. *Front. Immunol.* **2017**, *8*, No. 1489.
(18) Inestrosa, N. C.; Alvarez, A.; Pérez, C. A.; Moreno, R. D.; Vicente, M.; Linker, C.; Casanueva, O. I.; Soto, C.; Garrido, J. Acetylcholinesterase Accelerates Assembly of Amyloid-β-Peptides into Alzheimer's Fibrils: Possible Role of the Peripheral Site of the Enzyme. *Neuron* **1996**, *16*, 881−891.
(19) Geula, C.; Mesulam, M. M. Cholinergic Systems and related neuropathological predilection partners in AD. In *Alzheimer Disease*; Raven Press: New York, 1993.
(20) Francis, P. T.; Palmer, A. M.; Snape, M.; Wilcock, G. K. The cholinergic hypothesis of Alzheimer's disease: a review of progress. *J. Neurol., Neurosurg. Psychiatry* **1999**, *66*, 137.
(21) Varadarajan, S.; Yatin, S.; Aksenova, M.; Butterfield, D. A. Review: Alzheimer's Amyloid β-Peptide-Associated Free Radical Oxidative Stress and Neurotoxicity. *J. Struct. Biol.* **2000**, *130*, 184−208.
(22) Tamagno, E.; Parola, M.; Bardini, P.; Piccini, A.; Borghi, R.; Guglielmotto, M.; Santoro, G.; Davit, A.; Danni, O.; Smith, M. A.; Perry, G.; Tabaton, M. β-Site APP cleaving enzyme up-regulation induced by 4-hydroxynonenal is mediated by stress-activated protein kinases pathways. *J. Neurochem.* **2005**, *92*, 628−636.
(23) Smith, M. A.; Rottkamp, C. A.; Nunomura, A.; Raina, A. K.; Perry, G. Oxidative stress in Alzheimer's disease. *Biochim. Biophys. Acta, Mol. Basis Dis.* **2000**, *1502*, 139−144.
(24) Bartus, R. T.; Dean, R. L.; Beer, B.; Lippa, A. S. The cholinergic hypothesis of geriatric memory dysfunction. *Science* **1982**, *217*, 408.
(25) Arvidsson, U.; Riedl, M.; Elde, R.; Meister, B. Vesicular acetylcholine transporter (VAChT) protein: A novel and unique marker for cholinergic neurons in the central and peripheral nervous systems. *J. Comp. Neurol.* **1997**, *378*, 454−467.
(26) Morán, M. A.; Mufson, E. J.; Gómez-Ramos, P. Colocalization of cholinesterases with β amyloid protein in aged and Alzheimer's brains. *Acta Neuropathol.* **1993**, *85*, 362−369.
(27) Alvarez, A.; Bronfman, F.; Pérez, C. A.; Vicente, M.; Garrido, J.; Inestrosa, N. C. Acetylcholinesterase, a senile plaque component, affects the fibrillogenesis of amyloid-β-peptides. *Neurosci. Lett.* **1995**, *201*, 49−52.
(28) Inestrosa, N. C.; Dinamarca, M. C.; Alvarez, A. Amyloid-cholinesterase interactions. Implications for Alzheimer's disease. *FEBS J.* **2008**, *275*, 625−632.
(29) Alvarez, A.; Opazo, C.; Alarcon, R.; Garrido, J.; Inestrosa, N. C. Acetylcholinesterase promotes the aggregation of amyloid-β-peptide fragments by forming a complex with the growing fibrils. *J. Mol. Biol.* **1997**, *272*, 348−361.
(30) Racchi, M.; Mazzucchelli, M.; Porrello, E.; Lanni, C.; Govoni, S. Acetylcholinesterase inhibitors: novel activities of old molecules. *Pharmacol. Res.* **2004**, *50*, 441−451.
(31) Pohanka, M. Acetylcholinesterase inhibitors: a patent review (2008 − present). *Expert Opin. Ther. Pat.* **2012**, *22*, 871−886.
(32) McGleenon, B. M.; Dynan, K. B.; Passmore, A. P. Acetylcholinesterase inhibitors in Alzheimer's disease. *Br. J. Clin. Pharmacol.* **1999**, *48*, 471−480.
(33) Cummings, J. L. Cholinesterase Inhibitors: A New Class of Psychotropic Compounds. *Am. J. Psychiatry* **2000**, *157*, 4−15.
(34) Anand, P.; Singh, B. A review on cholinesterase inhibitors for Alzheimer's disease. *Arch. Pharmacal Res.* **2013**, *36*, 375−399.
(35) Perry, E. K.; Curtis, M.; Dick, D. J.; Candy, J. M.; Atack, J. R.; Bloxham, C. A.; Blessed, G.; Fairbairn, A.; Tomlinson, B. E.; Perry, R. H. Cholinergic correlates of cognitive impairment in Parkinson's disease: comparisons with Alzheimer's disease. *J. Neurol., Neurosurg. Psychiatry* **1985**, *48*, 413.
(36) Perry, E. K.; Tomlinson, B. E.; Blessed, G.; Bergmann, K.; Gibson, P. H.; Perry, R. H. Correlation of cholinergic abnormalities with senile plaques and mental test scores in senile dementia. *Br. Med. J.* **1978**, *2*, 1457.

https://dx.doi.org/10.1021/acs.jcim.0c00463
J. Chem. Inf. Model. XXXX, XXX, XXX−XXX

(37) Mirjana, B. C.; Danijela, Z. K.; Tamara, D. L.-P.; Aleksandra, M. B.; Vesna, M. V. Acetylcholinesterase Inhibitors: Pharmacology and Toxicology. *Curr. Neuropharmacol.* **2013**, *11*, 315−335.
(38) Tayeb, H. O.; Yang, H. D.; Price, B. H.; Tarazi, F. I. Pharmacotherapies for Alzheimer's disease: Beyond cholinesterase inhibitors. *Pharmacol. Ther.* **2012**, *134*, 8−25.
(39) Bolognesi, M. L.; Cavalli, A.; Valgimigli, L.; Bartolini, M.; Rosini, M.; Andrisano, V.; Recanatini, M.; Melchiorre, C. Multi-Target-Directed Drug Design Strategy: From a Dual Binding Site Acetylcholinesterase Inhibitor to a Trifunctional Compound against Alzheimer's Disease. *J. Med. Chem.* **2007**, *50*, 6446−6449.
(40) Xie, Y.; Yang, W.; Chen, X.; Xiao, J. Inhibition of flavonoids on acetylcholine esterase: binding and structure-activity relationship. *Food Funct.* **2014**, *5*, 2582−2589.
(41) Wang, X.; Cao, J.; Wu, Y.; Wang, Q.; Xiao, J. Flavonoids, Antioxidant Potential, and Acetylcholinesterase Inhibition Activity of the Extracts from the Gametophyte and Archegoniophore of *Marchantia polymorpha* L. *Molecules* **2016**, *21*, No. 360.
(42) Satheesh Kumar, N.; Mukherjee, P. K.; Bhadra, S.; Saha, B. P. Acetylcholinesterase enzyme inhibitory potential of standardized extract of Trigonella foenum graecum L and its constituents. *Phytomedicine* **2010**, *17*, 292−295.
(43) Mukherjee, P. K.; Kumar, V.; Mal, M.; Houghton, P. J. Acetylcholinesterase inhibitors from plants. *Phytomedicine* **2007**, *14*, 289−300.
(44) Marco, J. L.; de los Rı′os, C.; Carreiras, M. C.; Baños, J. E.; Badía, A.; Vivas, N. M. Synthesis and acetylcholinesterase/butyrylcholinesterase inhibition activity of new tacrine-like analogues. *Bioorg. Med. Chem.* **2001**, *9*, 727−732.
(45) Francisco, W.; Pivatto, M.; Danuello, A.; Regasini, L. O.; Baccini, L. R.; Young, M. C. M.; Lopes, N. P.; Lopes, J. L. C.; Bolzani, V. S. Pyridine Alkaloids from Senna multijuga As Acetylcholinesterase Inhibitors. *J. Nat. Prod.* **2012**, *75*, 408−413.
(46) Barreiro, E. J.; Camara, C. A.; Verli, H.; Brazil-Más, L.; Castro, N. G.; Cintra, W. M.; Aracava, Y.; Rodrigues, C. R.; Fraga, C. A. M. Design, Synthesis, and Pharmacological Profile of Novel Fused Pyrazolo[4,3-d]pyridine and Pyrazolo[3,4-b][1,8]naphthyridine Isosteres: A New Class of Potent and Selective Acetylcholinesterase Inhibitors. *J. Med. Chem.* **2003**, *46*, 1144−1152.
(47) Galgani, F.; Bocquene, G. In Vitro inhibition of acetylcholinesterase from four marine species by organophosphates and carbamates. *Bull. Environ. Contam. Toxicol.* **1990**, *45*, 243−249.
(48) Storm, J. E.; Rozman, K. K.; Doull, J. Occupational exposure limits for 30 organophosphate pesticides based on inhibition of red blood cell acetylcholinesterase. *Toxicology* **2000**, *150*, 1−29.
(49) Guyton, K. Z.; Loomis, D.; Grosse, Y.; El Ghissassi, F.; Benbrahim-Tallaa, L.; Guha, N.; Scoccianti, C.; Mattock, H.; Straif, K. Carcinogenicity of tetrachlorvinphos, parathion, malathion, diazinon, and glyphosate. *Lancet Oncol.* **2015**, *16*, 490−491.
(50) Cabello, G.; Valenzuela, M.; Vilaxa, A.; Durán, V.; Rudolph, I.; Hrepic, N.; Calaf, G. A rat mammary tumor model induced by the organophosphorous pesticides parathion and malathion, possibly through acetylcholinesterase inhibition. *Environ. Health Perspect.* **2001**, *109*, 471−479.
(51) Sakayanathan, P.; Loganathan, C.; Kandasamy, S.; Ramanna, R. V.; Poomani, K.; Thayumanavan, P. In vitro and in silico analysis of novel astaxanthin-s-allyl cysteine as an inhibitor of butyrylcholinesterase and various globular forms of acetylcholinesterases. *Int. J. Biol. Macromol.* **2019**, *140*, 1147−1157.
(52) Chen, K.-L.; Gan, L.; Wu, Z.-H.; Qin, J.-F.; Liao, W.-X.; Tang, H. 4- Substituted sampangine derivatives: Novel acetylcholinesterase and β-myloid aggregation inhibitors. *Int. J. Biol. Macromol.* **2018**, *107*, 2725−2729.
(53) Topal, F.; Gulcin, I.; Dastan, A.; Guney, M. Novel eugenol derivatives: Potent acetylcholinesterase and carbonic anhydrase inhibitors. *Int. J. Biol. Macromol.* **2017**, *94*, 845−851.
(54) Hamulakova, S.; Janovec, L.; Soukup, O.; Jun, D.; Kuca, K. Synthesis, in vitro acetylcholinesterase inhibitory activity and molecular docking of new acridine-coumarin hybrids. *Int. J. Biol. Macromol.* **2017**, *104*, 333−338.
(55) Kuppusamy, A.; Arumugam, M.; George, S. Combining in silico and in vitro approaches to evaluate the acetylcholinesterase inhibitory profile of some commercially available flavonoids in the management of Alzheimer's disease. *Int. J. Biol. Macromol.* **2017**, *95*, 199−203.
(56) Pushpakom, S.; Iorio, F.; Eyers, P. A.; Escott, K. J.; Hopper, S.; Wells, A.; Doig, A.; Guilliams, T.; Latimer, J.; McNamee, C.; Norris, A.; Sanseau, P.; Cavalla, D.; Pirmohamed, M. Drug repurposing: progress, challenges and recommendations. *Nat. Rev. Drug Discovery* **2019**, *18*, 41.
(57) Wishart, D. S.; Feunang, Y. D.; Guo, A. C.; Lo, E. J.; Marcu, A.; Grant, J. R.; Sajed, T.; Johnson, D.; Li, C.; Sayeeda, Z.; Assempour, N.; Iynkkaran, I.; Liu, Y.; Maciejewski, A.; Gale, N.; Wilson, A.; Chin, L.; Cummings, R.; Le, D.; Pon, A.; Knox, C.; Wilson, M. DrugBank 5.0: a major update to the DrugBank database for 2018. *Nucleic Acids Res.* **2018**, *46*, D1074−D1082.
(58) Law, V.; Knox, C.; Djoumbou, Y.; Jewison, T.; Guo, A. C.; Liu, Y.; Maciejewski, A.; Arndt, D.; Wilson, M.; Neveu, V.; Tang, A.; Gabriel, G.; Ly, C.; Adamjee, S.; Dame, Z. T.; Han, B. H.; Zhou, Y.; Wishar, D. S. DrugBank 4.0: shedding new light on drug metabolism. *Nucleic Acids Res.* **2014**, *42*, D1091−D1097.
(59) Bar-On, P.; Millard, C. B.; Harel, M.; Dvir, H.; Enz, A.; Sussman, J. L.; Silman, I. Kinetic and Structural Studies on the Interaction of Cholinesterases with the Anti-Alzheimer Drug Rivastigmine. *Biochemistry* **2002**, *41*, 3555−3564.
(60) Bietz, S.; Urbaczek, S.; Schulz, B.; Rarey, M. Protoss: a holistic approach to predict tautomers and protonation states in protein-ligand complexes. *Chem. Soc. Rev.* **2014**, *6*, No. 12.
(61) Pettersen, E. F.; Goddard, T. D.; Huang, C. C.; Couch, G. S.; Greenblatt, D. M.; Meng, E. C.; Ferrin, T. E. UCSF Chimera—A visualization system for exploratory research and analysis. *J. Comput. Chem.* **2004**, *25*, 1605−1612.
(62) Stroganov, O. V.; Novikov, F. N.; Stroylov, V. S.; Kulkov, V.; Chilov, G. G. Lead Finder: An Approach To Improve Accuracy of Protein−Ligand Docking, Binding Energy Estimation, and Virtual Screening. *J. Chem. Inf. Model.* **2008**, *48*, 2371−2385.
(63) Novikov, F. N.; Stroylov, V. S.; Stroganov, O. V.; Chilov, G. G. Improving performance of docking-based virtual screening by structural filtration. *J. Mol. Model.* **2010**, *16*, 1223−1230.
(64) Novikov, F. N.; Stroylov, V. S.; Zeifman, A. A.; Stroganov, O. V.; Kulkov, V.; Chilov, G. G. Lead Finder docking and virtual screening evaluation with Astex and DUD test sets. *J. Comput.-Aided Mol. Des.* **2012**, *26*, 725−735.
(65) Wolber, G.; Langer, T. LigandScout: 3-D Pharmacophores Derived from Protein-Bound Ligands and Their Use as Virtual Screening Filters. *J. Chem. Inf. Model.* **2005**, *45*, 160−169.
(66) Ge, H.; Wang, Y.; Zhao, W.; Lin, W.; Yan, X.; Xu, J. Scaffold hopping of potential anti-tumor agents by WEGA: a shape-based approach. *Med. Chem. Commun.* **2014**, *5*, 737−741.
(67) Tsai, T.-Y.; Chang, K.-W.; Chen, C. Y.-C. iScreen: world's first cloud-computing web server for virtual screening and de novo drug design based on TCM database@Taiwan. *J. Comput.-Aided Mol. Des.* **2011**, *25*, 525−531.
(68) Ruggiu, F.; Marcou, G.; Varnek, A.; Horvath, D. ISIDA Property-Labelled Fragment Descriptors. *Mol. Inf.* **2010**, *29*, 855−868.
(69) Todeschini, R.; Ballabio, D.; Consonni, V.; Manganaro, A.; Mauri, A. Canonical Measure of Correlation (CMC) and Canonical Measure of Distance (CMD) between sets of data. Part 1. Theory and simple chemometric applications. *Anal. Chim. Acta* **2009**, *648*, 45−51.
(70) Ellman, G. L.; Courtney, K. D.; Andres, V.; Featherstone, R. M. A new and rapid colorimetric determination of acetylcholinesterase activity. *Biochem. Pharmacol.* **1961**, *7*, 88−95.
(71) Senol, F. S.; Ślusarczyk, S.; Matkowski, A.; Pérez-Garrido, A.; Girón-Rodríguez, F.; Cerón-Carrasco, J. P.; den-Haan, H.; Peña-García, J.; Pérez-Sánchez, H.; Domaradzki, K.; Orhan, I. E. Selective in vitro and in silico butyrylcholinesterase inhibitory activity of

https://dx.doi.org/10.1021/acs.jcim.0c00463
J. Chem. Inf. Model. XXXX, XXX, XXX−XXX

777 diterpenes and rosmarinic acid isolated from Perovskia atriplicifolia
778 Benth. and Salvia glutinosa L. *Phytochemistry* **2017**, *133*, 33−44.
779 (72) Pantsar, T.; Poso, A. Binding Affinity via Docking: Fact and
780 Fiction. *Molecules* **2018**, *23*, No. 1899.
781 (73) Davies, P.; Maloney, A. J. F. Selective Loss of Central
782 Cholinergic Neurons in Alzheimer's Disease. *Lancet* **1976**, *308*, 1403.
783 (74) Mukherjee, P. K.; Kumar, V.; Houghton, P. J. Screening of
784 Indian medicinal plants for acetylcholinesterase inhibitory activity.
785 *Phytother. Res.* **2007**, *21*, 1142−1145.
786 (75) Galimberti, D.; Scarpini, E. Old and new acetylcholinesterase
787 inhibitors for Alzheimer's disease. *Expert Opin. Invest. Drugs* **2016**, *25*,
788 1181−1187.
789 (76) Pisani, L.; Farina, R.; Catto, M.; Iacobazzi, R. M.; Nicolotti, O.;
790 Cellamare, S.; Mangiatordi, G. F.; Denora, N.; Soto-Otero, R.;
791 Siragusa, L.; Altomare, C. D.; Carotti, A. Exploring Basic Tail
792 Modifications of Coumarin-Based Dual Acetylcholinesterase-Mono-
793 amine Oxidase B Inhibitors: Identification of Water-Soluble, Brain-
794 Permeant Neuroprotective Multitarget Agents. *J. Med. Chem.* **2016**,
795 *59*, 6791−6806.

https://dx.doi.org/10.1021/acs.jcim.0c00463
J. Chem. Inf. Model. XXXX, XXX, XXX−XXX